NANO LETTERS

LETTER

pubs.acs.org/NanoLett

Sulfur-Impregnated Disordered Carbon Nanotubes Cathode for Lithium−Sulfur Batteries

Juchen Guo, Yunhua Xu, and Chunsheng Wang*

Department of Chemical and Biomolecular Engineering University of Maryland, College Park, Maryland 20742, United States

Supporting Information

ABSTRACT: The commercialization of lithium−sulfur batteries is hindered by low cycle stability and low efficiency, which are induced by sulfur active material loss and polysulfide shuttle reaction through dissolution into electrolyte. In this study, sulfur-impregnated disordered carbon nanotubes are synthesized as cathode material for the lithium−sulfur battery. The obtained sulfur−carbon tube cathodes demonstrate superior cyclability and Coulombic efficiency. More importantly, the electrochemical characterization indicates a new stabilization mechanism of sulfur in carbon induced by heat treatment.

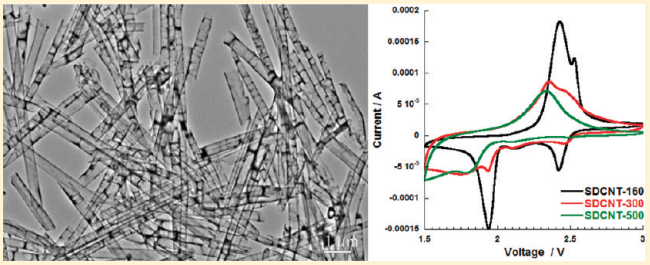

KEYWORDS: Disordered carbon nanotubes, lithium−sulfur batteries, sulfur impregnation, sulfur−carbon bonds

The emerging plug-in hybrid vehicle and electric vehicle technologies demand significant improvement of rechargeable battery technologies to achieve higher energy density. Despite the numerous advantages, the overall energy density of lithium ion batteries is limited by the low capacity of current cathode materials.[1−3] Therefore, rechargeable batteries beyond lithium ion have been extensively investigated as alternatives. Among them, a lithium−sulfur (Li−S) battery is an attractive technology for a number of desirable properties. Attributing to the 1675 mAh g^{-1} theoretical capacity of sulfur cathode, Li−S batteries have very high specific energy density (theoretically 2500 Wh kg^{-1}).[4] Moreover, Li−S batteries are made with abundant and nonpoisonous sulfur that is a common byproduct of the petroleum refining process. Despite the great promises, there still are a number of complex problems that need to be solved for the commercialization of Li−S batteries. Li−S batteries are based on the reversible redox reaction between lithium and sulfur with lithium sulfide (Li_2S) as the final product of sulfur reduction (discharge). During the redox reaction between lithium and sulfur, there are several intermediate reactions with intermediate products referred as lithium polysulfides (Li_2S_n).[5] Lithium polysulfides are electrical insulators so that in-depth discharge of sulfur could be difficult, leading to low utilization of sulfur and low rate capacity as the comment problems for Li−S batteries.[6] This problem could be alleviated by using electrolyte with polar organic solvents including 1,3-dioxolane (DOL), dimethoxyethane (DME), and tetra(ethylene glycol) dimethyl ether (TEGDME) that could dissolve lithium polysulfides to some extent.[7−12] These solvents can dissolve lithium polysulfides, especially the high order polysulfides with $n > 4$,[3] making sulfur accessible for more complete reduction. However, using these solvents could cause a more serious problem for Li−S batteries: The dissolved lithium polysulfides can diffuse to the anode to directly react to the Li metal, forming lower order polysulfides including insoluble Li_2S_2 and Li_2S, which will deposit on the Li anode. The soluble S_{n-x}^{2-} lower order polysulfides will diffuse back to the cathode due to concentration gradient and be reoxidized to S_n^{2-} higher order forms, creating the so-called internal "shuttle mechanism".[13,14] Therefore, the dissolution of polysulfides led to not only fast capacity fading due to the Li_2S_2/Li_2S deposition on the anode but also severe low Coulombic efficiency due to the shuttle mechanism, i.e., charge capacity higher than the corresponding discharge capacity, especially at low charge/discharge rate.[15] It is well recognized nowadays that the problem of polysulfide dissolution has to be solved to realize Li−S technology.

Current methodologies to alleviate this problem could be sorted into two categories: The first one was to physically restrain polysulfide dissolution using barrier materials. The physical restraint methods included carbon coating on sulfur,[16] high surface-area carbon additives,[17−20] and polymeric electrolytes.[21,22] The most promising physical restraint methods seemed to be incorporating sulfur into mesoporous host (mostly carbon) structures to contain the polysulfides.[23−29] The obvious advantage of mesoporous structures is their small pores size and large overall pore volume. However, if the sulfur in the mesopores could still be accessed by electrolyte in which polysulfides could be dissolved, the active materials loss could only be alleviated, but not eliminated. This could be the reason that extended cycle life (~100 cycles) tests with stable capacity retention and high Coulombic efficiency were rarely reported. The second methodology was to use mesoporous silica as intermediate polysulfides absorber through weak bonding,[30] or using metal (such as copper and nickel) as sulfur absorber by forming metal−S alloys.[31] It was demonstrated that using a nickel

Received: July 6, 2011
Revised: August 23, 2011
Published: September 19, 2011

current collector could improve the cyclability of sulfur cathode.[32] With simple mixture of sulfur, carbon black, and PVDF incorporated in nickel foam, superior cyclability could be achieved.[32] The true mechanism of such a good cyclability could be attributed to the formation of nickel sulfide, which could be speculated from the reported slope-shaped charge/discharge curves showing characteristic nickel sulfide behavior.[31] However, the metal absorber significantly decreased the specific capacity due to the added metal mass. Demonstrated by previous studies, it is clear that both methodologies have limitations. The ideal scenario is that the sulfur should be locked and bound in certain carbon structures and not be in direct contact with the electrolyte. Therefore, the redox reaction between sulfur and Li mostly takes place through a carbon barrier that is both electron and Li ion conductive, without direct contact with electrolyte. Also, the cyclic octatomic S_8 molecule should be broken into smaller structures (such as S_6 or S_2) so that soluble high-order polysulfides could be eliminated even if the liquid electrolyte penetrates into carbon and reacts with sulfur. Unfortunately, these perspectives have not been characterized to date.

In this study, we validated the above hypothesis by carrying out a new method of impregnating sulfur into disordered carbon nanotubes (DCNTs) as cathode material for Li−S batteries. The synthesis of sulfur-impregnated DCNTs (SDCNTs) is illustrated in Figure S1 in the Supporting Information. The DCNTs were prepared by a template wetting technique using commercial anodic aluminum oxide (AAO) membranes (Whatman International Ltd.) as the template.[33] The pore size and thickness of the AAO membrane are 200 and 70 μm, respectively. To fabricate the DCNTs, 1 drop of 10 wt % polyacrylonitrile (PAN, molecular weight 150000 g mol^{-1}, Sigma-Aldrich) solution in DMF was dropped on the aluminum foil, and an AAO membrane was placed on top of the PAN solution. The membrane wetting by drawing the PAN solution into the pores due to capillary force could be visually observed. The wetted AAO membrane was then dried at 150 °C in a vacuum oven overnight. After drying, the PAN filled AAO membrane was peeled off from the aluminum foil. The PAN thin film on the bottom of the AAO membrane was removed by oxygen reactive ion etching. During the carbonization process, the PAN incorporated AAO membrane was first heated at 250 °C in air for 30 min to stabilize the PAN and then heated at 600 °C for an hour to carbonize the PAN. The heating rate was 2 °C min^{-1} in the stabilization and 10 °C min^{-1} in the carbonization. After being naturally cooled to room temperature, the AAO template was removed by dissolving in 1 M NaOH aqueous solution. The obtained DCNTs array was washed with abundant distilled water. The typical sulfur impregnation process is as follows: 0.1 g of sublimed sulfur power (Sigma-Aldrich) was evenly put on the top of a 0.05 g DCNTs array. One milliliter of CS_2 was dripped on the sulfur to dissolve it enabling the impregnation. The sample was dried in a fume hood and then put in quartz tubes that were sealed under vacuum. The sulfur impregnation was further carried out by heating the SDCNTs in the vacuum-sealed quartz tube under three different temperatures: SDCNT-160 was obtained by being heated at 160 °C for 10 h. SDCNT-300 and SDCNT-500 were obtained by being further heated at 300 and 500 °C for 3 h more, respectively. The disordered DCNTs possess graphitic clusters and amorphous carbon structures that were accessible by sulfur vapor, thus serving as the sulfur host and preventing liquid electrolyte penetration. Most of the previous studies incorporated sulfur into porous carbon by heating the sulfur−carbon mixture at around 155 °C under the protection of inert gas. The reason was

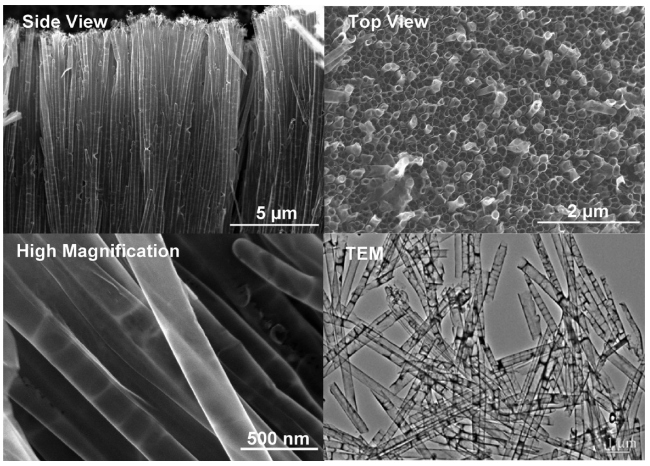

Figure 1. SEM and TEM images of the disordered carbon nanotubes prepared by the template wetting method.

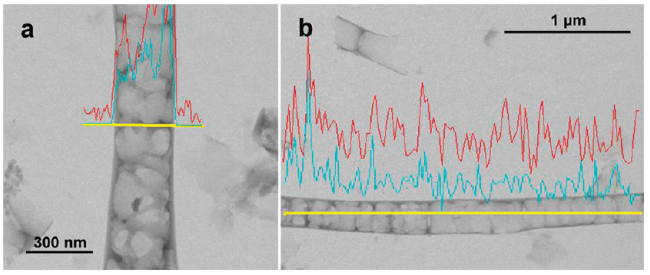

Figure 2. TEM images and EDS line scanning of the sulfur impregnated disordered carbon nanotubes at 300 °C (a) along the cross section and (b) along the axis direction. Carbon signal is red and sulfur signal is blue.

that elemental sulfur (S_8) became liquid and had the lowest viscosity at 155 °C so that the liquid sulfur could infuse into the host structure.[24] A potential problem of this method was that liquid electrolyte could still reach into the sites where liquid sulfur could diffuse into. On the contrary, sulfur can be vaporized at elevated temperature in vacuum so that sulfur vapor could intercalate into carbon voids and even into graphite layers of graphitic clusters depending on temperature.[34] Therefore, we heated the sulfur-impregnated DCNTs at 160, 300, and 500 °C in vacuum-sealed quartz tubes (denoted as SDCNT-160, SDCNT-300, and SDCNT-500, respectively).

Two-electrode coin cells with lithium foil as the counter electrode were assembled in an argon-filled glovebox for the electrochemistry analysis. Electrolyte consisting of 1 M bis-(trifluoromethane)sulfonimide lithium salt (LiTFSI, Sigma-Aldrich) in TEGDME (Sigma-Aldrich) was used with a microporous membrane separator (Celgard 3501). The cells were charged and discharged with different cycling currents between 1.5 and 3 V (vs Li/Li+) using an Arbin battery test station. The cyclic voltammetry measurements were carried out with a scan rate of 0.1 mV s^{-1} on a Solartron SI1287/1260 analyzer.

Figure 1 shows the scanning electron microscopy (SEM) and transmission electron microscopy (TEM) images of the as-prepared DCNTs. (A high-resolution TEM image is shown in Figure S2 in the Supporting Information). From the side view and top view, it can be seen that the DCNTs bundled together as an array. The high magnification SEM and TEM images show the

dx.doi.org/10.1021/nl202297p |Nano Lett. 2011, 11, 4288–4294

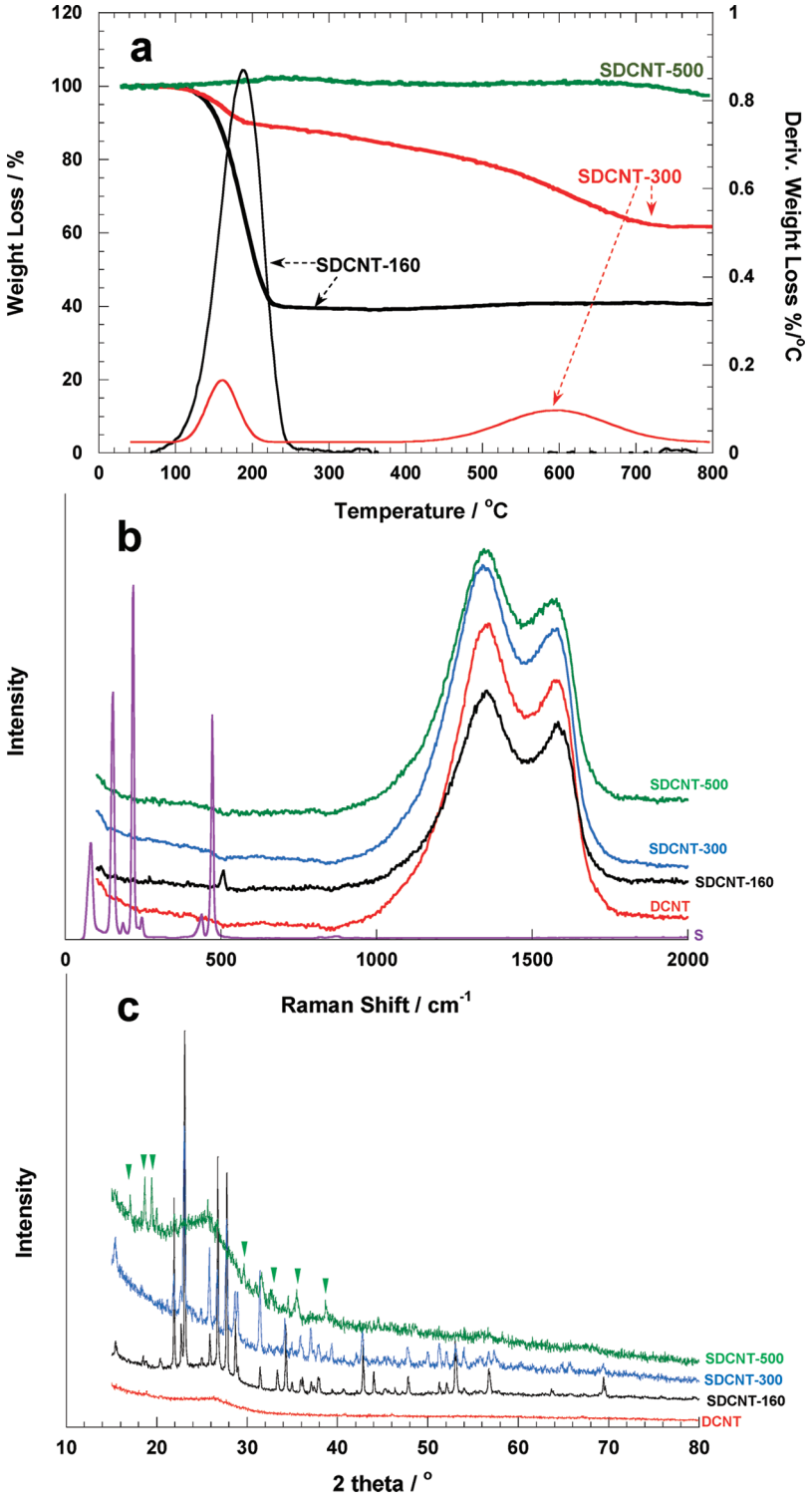

Figure 3. (a) TGA curve of sulfur impregnated disordered carbon nanotubes. (b) Raman spectra of pure sulfur, DCNT, SDCNT-160, SDCNT-300, and SDCNT-500. (c) XRD spectra of sulfur impregnated in DCNTs.

diameter of the DCNTs is about 200 nm, and the thickness of the carbon wall is uniform. Figure 2 shows the transmission electron microscopy (TEM) images of the sulfur-impregnated DCNTs at 300 °C. Energy-dispersive X-ray spectroscopy (EDS) was used for the elemental analysis. Figure 2a is the EDS line scanning along the cross section of the sulfur-impregnated DCNT, and Figure 2b is the EDS line scanning along the axis of the tube. The EDS spectra proved the existence of sulfur in the DCNTs, and the consistent signal indicated the distribution of the sulfur was uniform. Thermogravimetric analysis (TGA) was performed in a nitrogen environment to determine the sulfur content and the mechanism of sulfur incorporation in DCNTs. Since the weight loss in TGA analysis is due to the evaporation of sulfur, the TGA pattern is an effective indication of sulfur

dx.doi.org/10.1021/nl202297p |*Nano Lett.* 2011, 11, 4288–4294

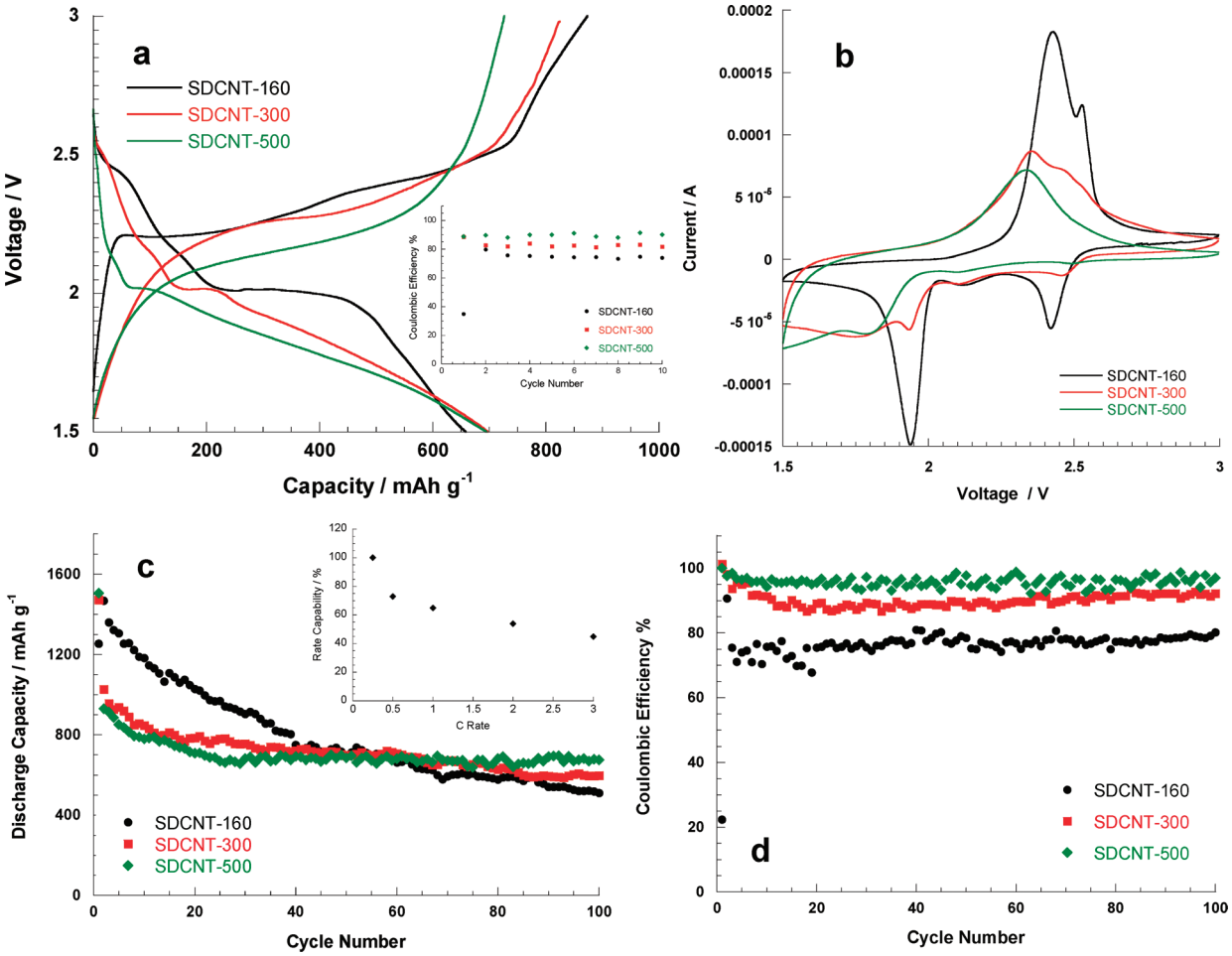

Figure 4. (a) Discharge/charge curves of the second cycles and Coulombic efficiency under 10 mA g^{-1}. (b) Cyclic voltammetry curves of the second cycles at scan rate of 0.1 mV s^{-1}. (c) Cycling stability and (d) Coulombic efficiencies of SDCNTs cathodes.

absorption strength in the carbon structures and possible sulfur−carbon bonding.[25] It could be expected that the evaporation temperature of sulfur intercalated in smaller voids (such as micropores) should be higher than that of sulfur in larger voids (such as mesopores).[25] As the TGA curves shown in Figure 3a, the SDCNT-160 only showed one sulfur evaporation peak at 200 °C, then its weight loss stopped at 220 °C. This single sulfur evaporation peak may indicate that sulfur in SDCNT-160 is mainly located in relatively large scale voids or on the surface of the DCNTs. The sulfur content in SDCNT-160 could be determined as 60 wt %. The SDCNT-300 showed a similar sulfur evaporation peak at 180 °C with relatively smaller magnitude. After that, its weight continued to gradually decrease and showed another broad decomposition peak at 600 °C. Its weight loss stopped at 700 °C, and the sulfur content in SDCNT-300 could be determined as 40 wt %. These two sulfur evaporation peaks may suggest that beside in large voids or on surface, a large portion of sulfur in SDCNT-300 is intercalated in the smaller voids such as micropores in amorphous carbon. The TGA of SDCNT-500 did not show any significant weight loss until 700 °C, suggesting a strong bonding between sulfur and carbon (chemisorption of S in carbon)[34] by possible sulfur intercalation into graphitic cluster and defects in SDCNT-500 driven by higher temperature at 500 °C. It was reported that at temperature above 400 °C, sulfur could be intercalated into graphene layer of graphite.[35,36] The absence of sulfur evaporation peaks at 180−200 and 600 °C also indicates that very little sulfur exists in large voids or on the surface of SDCNT-500 where liquid electrolytes can access during charge/discharge cycles. The sulfur content in SDCNT-500 was determined as 40 wt % by EDS elemental analysis (EDS spectra is shown in Figure S3 and the element composition is shown in Table S1 in the Supporting Information) due to the lack of weight loss in TGA.

To better understand the interaction between sulfur and carbon, the structures of SDCNT with and without sulfur were characterized using Raman spectroscopy as shown in Figure 3b. The Raman spectrum of pure DCNTs showed a typical pattern of partially graphitized carbon. Two main peaks are seen in the spectrum taken from DCNTs, the G peak and the D peak. The G peak at around 1580 cm^{-1} is due to a bond stretching vibration of a pair of sp_2 sites corresponding to graphitic cluster lattice vibration mode with E_{2g} symmetry. The D peak at 1350 cm^{-1} is due to an A_{1g} breathing vibration of a 6-fold aromatic ring that is activated by disordered carbon. The relative intensity of the D band (I_D) and G band (I_G) in Raman spectrum provides the degree of graphitization and the size of any graphitic clusters present in disordered carbon.[37] The I_D is higher than I_G in the spectrum of pure DCNTs, indicating that DCNTs have a structure with a fraction of graphitic cluster dispersed in disordered carbon. However, the sulfur-impregnated DCNTs

dx.doi.org/10.1021/nl202297p |*Nano Lett.* 2011, 11, 4288–4294

samples did not show noticeable difference from the pure carbon tubes. Only SDCNT-160 showed a small peak at 500 cm^{-1}, probably indicating some sulfur residue. For further characterization, X-ray diffraction (XRD) analysis was also conducted on the SDCNT samples as shown in Figure 3c. The SDCNT-160 shows an XRD pattern consistent with elemental sulfur (S_8). The XRD pattern of SDCNT-300 is slightly different from SDCNT-160 with absence of a few peaks. A more interesting observation is that SDCNT-500 demonstrates a very different XRD pattern compared with the other two. The new peaks in the SDCNT-500 sample that are not in the other two are marked in the XRD pattern. Moreover, the new peaks in the SDCNT-500 XRD pattern could not be identified as any known compound, and we are currently working on indexing these peaks.

Carbon−sulfur bonding and sulfur structure in carbon (other than S_8) will change the equilibrium potential of S−Li reactions and the electrochemical lithiation/delithiation capacity. Therefore, the equilibrium potential versus capacity (Li composition) of SDCNT cathodes is a powerful indicator to detect the C−S bond and S−Li reaction mechanism. The equilibrium potentials of SDCNTs versus Li were estimated by their second charge/discharge curves at a very low current density of 10 mA g^{-1} (0.0125C, i.e., ∼80 h discharge and ∼80 h discharge) which was much lower than the required high current to prevent the polysulfide shuttle mechanism proposed by Mikhaylik and Akridge.[14] Figure 4a shows the second charge/discharge curves of three SDCNT cathodes at 0.0125C rate. Three plateaus are clearly shown in the discharge curve of SDCNT-160 at 2.45, 2.15, and 2.05 V, corresponding to the elemental sulfur (S_8) reduction to S_6^{2-}, S_4^{2-}, and S_2^{2-} (or S^{2-}), respectively. The reverse reactions were also demonstrated in the oxidation process with two potential plateaus in the charge curve. It is clear that the SDCNT-160 demonstrated typical sulfur cathode charge/discharge behavior and indicating that sulfur existed as S_8 in SDCNT-160, which produced soluble polysulfides and resulted in a relatively low Coulombic efficiency (∼75% shown in the inset) due to the partial shuttle reaction. On the contrary, the charge/discharge curve of SDCNT-300 and SDCNT-500 cathodes showed significantly different behavior. The first potential plateau at 2.45 V due to reduction from S_8 to S_6^{2-} and the second potential plateau at 2.2 V due to reduction from S_6^{2-} to S_4^{2-} are significantly reduced for SDCNT-300 and almost eliminated for SDCNT-500. This is a strong indication that the reaction route of $S_8 \rightarrow S_6^{2-} \rightarrow S_4^{2-}$ was suppressed in these two cathodes with increased heating temperature. It indicates that the form of sulfur in DCNTs changed from S_8 to S_6 and S_2 when heating temperature increased from 160 to 500 °C in vacuum. This finding is consistent with previous reported results.[38] It was reported that the sulfur vapor at 200 °C in vacuum is in forms of S_8 (76.5 wt %) and S_6 (23.5 wt %) rings.[39] At 600 °C, sulfur vapor possesses a significant fraction of S_6 (58.8 wt %) and S_2 (16.4 wt %) molecules.[40] The diameter of S_8 ranges from 7.6 to 8.4 Å depending on whether the molecule exists as a ring or a chain. The small S_6 (6.9 Å) and S_2 (5.2 Å) molecules are more reactive because they possess a greater fraction of sulfur terminal atom.[41] Their small size and strong bonding with carbon can more easily diffuse into the small voids and even intercalate into the graphite cluster.[38] Therefore, the equilibrium potential versus capacity curves in Figure 4a indicate that sulfur may mainly exist as S_8 in SDCNT-160; S_6, S_2, and a small portion of S_8 in SDCNT-300; and S_6 and S_2 with strong C−S bonding in defects and graphite layers in SDCNT-500. The strong bonding between S and C in SDCNT-300 and SDCNT-500 is evidenced by the shortened the capacity at a potential plateau of 2.05 V, followed by a slope-shaped curve. Similar to Ni−S alloy, the bond between sulfur and carbon in these two electrodes changed the potential of reaction route of $S_4^{2-} \rightarrow S_2^{2-} \rightarrow S^{2-}$ from a plateau to a sloped shape, which is consistent with their cyclic voltammetry characterization as detailed in the next paragraph. Also as shown in the inset of Figure 4a, the Coulombic efficiencies of SDCNTs cathodes at 0.0125C are approximately 75% (except the first cycle), 82%, and 91% for SDCNT-160, SDCNT-300, and SDCNT-500, respectively, indicating that liquid electrolyte penetrated into large voids of SDCNTs and inducing shuttle reaction if sulfur existed in the voids. The electrochemical analysis from Figure 4a strongly supports the findings from the TGA analysis in Figure 3a.

The electrochemical reaction mechanism of the SDCNTs cathodes was more clearly revealed using cyclic voltammetry (CV). The CV scan was performed on the SDCNT cathodes between 3.0 and 1.5 V using 0.1 mV s^{-1} scan rate (∼20 times faster than the low current charging/discharging in Figure 4a). Their CV curves of the second cycles are plotted in Figure 4b. The CV curve of the SDCNT-160 demonstrated typical sulfur cathode CV behavior:[42] the three cathodic peaks indicated the elemental sulfur (S_8) reduction to S_6^{2-}, S_4^{2-}, and S_2^{2-} (or S^{2-}), respectively. Two oxidation reaction peaks were observed: the first peak was associated with the formation of Li_2S_n ($n > 2$), and the second peak corresponded to the formation of Li_2S_n ($n \leq 2$).[29] The reaction of SDCNT-160 was consistent with the conventional redox reaction between S_8 and Li as its CV curve indicated.[29,42] On the contrary, the CV curve of SDCNT-300 cathode showed significant different behavior. The magnitudes of the three previously mentioned reduction peaks were greatly reduced. More interestingly, SDCNT-300 showed a new broad peak at 1.8 V, which was lower than the potential of $S_4^{2-} \rightarrow S_2^{2-}$ reaction at 1.95 V. Also, only two oxidation peaks could be identified. The 1.8 V peak in the SDCNT-500 cathode became broader and the other two reduction peaks were further reduced compared with SDCNT-300. This observation indicated that the electrochemical reactions in SDCNT-300 and SDCNT-500 are dominated by the new reaction represented by the new peak at 1.8 V, and the conventional intermediate reactions were greatly suppressed. Moreover, the conventional intermediate reactions were either significant reduced in SDCNT-300 or completely eliminated in SDCNT-500 within 20 charge/discharge cycles (Figures S5 and S6 in the Supporting Information). The new broad peak at 1.8 V in both SDCNT-300 and SDCNT-500 was possibly attributed to $S_2 \rightarrow S^{2-}$ reaction and the strong bonding between sulfur and carbon. The low current charge/discharge curves and the CV scan, combined with the TGA and XRD analysis, revealed a new mechanism to stabilize sulfur−carbon cathodes.

The cycle stability of the SDCNTs cathodes at 200 mA g^{-1} (0.25C) is shown in Figure 4c. The rate capability (ratio of capacity at nC to the capacity at 0.25C) of SDCNT-300 is also plotted as the inset of Figure 4c. Even all the SDCNT cathodes showed good cycle stability, the SDCNT-160 had the fastest capacity fading of 34.8% retention after 100 cycles. The SDCNT-300 cathode showed better stability of 53.3% retention after 100 cycles except the first one, and the SDCNT-500 cathode had the best performance among all three with 72.9% retention after 100 cycles except the first one: after 30 cycles, the capacity of SDCNT-500 stopped decreasing completely. The large capacity drop between the first and second cycle for SDCNT-300 and

dx.doi.org/10.1021/nl202297p |*Nano Lett.* 2011, 11, 4288–4294

SDCNT-500 could be attributed to the superficial sulfur deposited on the surface of disordered carbon nanotubes during the cooling process after the heating. These observations indicated that the heat treatment had a profound effect on the performance of SDCNTs cathodes. Although most of the sulfur was not in direct contact with liquid electrolyte in high-temperature SDCNTs cathodes, the Li ions could quickly diffuse through carbon and react to sulfur due to high diffusivity of Li ions in carbon. The fast Li diffusion in carbon was evidenced by the great rate capability of SDCNT-300. The capacity of SDCNT-300 at 3C could still reach 50% of capacity at 0.25C as shown in the insert in Figure 4c. The Coulombic efficiencies of SDCNT-160, SDCNT-300, and SDCNT-500 under 200 mA g^{-1} rate are plotted in Figure 4d. It clearly demonstrated that the Coulombic efficiency was improved with increased heating temperature. Especially for SDCNT-300 and SDCNT-500, their Coulombic efficiencies at 0.25C rate were averagely at 89% and 96% during 100 cycles, respectively. The 96% Coulombic efficiency of SDCNT-500 at 0.25C is the highest value in open literature for sulfur cathode. The elimination of the polysulfide shuttle mechanism in SDCNT-300 and SDCNT-500 cathodes indicated the possibility that the sulfur was incorporated in the voids/graphite layers in the partially graphitized DCNTs carbon structure, which could not be directly contacted by electrolyte. Also, the distinctly different CV and charge/discharge curves of SDCNT-300 and SDCNT-500 indicated possible sulfur−carbon bonding and existence of smaller sulfur structures (S_6 and S_2) induced by the heat treatment a in vacuum environment.

The continuous CV scan of SDCNT cathodes can also demonstrate their cycle stability, since the integrated area of the CV peak is equal to capacity. Representative CV curves from continuous scan of SDCNT-160, SDCNT-300, and SDCNT-500 are shown in Figures S4, S5, and S6 in the Supporting Information, respectively. It is clear that the capacity of SDCNT-160 decreases significantly from the second cycle to the 80th cycle. The continuous CV scan of SDCNT-300 clearly shows better capacity retention, and even better capacity retention of SDCNT-500 was demonstrated by its continuous CV scan.

In summary, the sulfur-impregnated DCNTs demonstrated great cycling stability and Coulombic efficiency as the cathode materials for Li−S batteries. We believe such improvement was induced by the high temperature heat treatment of SDCNTs in a vacuum environment. The hypothesis is that the vaporized sulfur can be incorporated into graphitized carbon layers and smaller voids/defects in amorphous carbon that liquid electrolyte cannot directly reach. Moreover, the heat treatment could break down the S_8 molecule to S_6 or S_2 and enable sulfur−carbon bonding so that the conventional Li−S_8 reaction with dissolvable polysulfide intermediate products might be altered. This hypothesis was indicated by the results of capacity retention, cyclic voltammetry, galvanostatic discharge/charge at low rate, TGA, and XRD presented in this study. It is specially worth to mention a latest study by Jayaprakash et al.[29] In their study, sulfur was incorporated into porous hollow carbon particles with their patented "sulfur vapor infusion" method. Such sulfur incorporated carbon particles demonstrated impressive cyclability and Coulombic efficiency. The authors claimed the great performance could be attributed to the incorporation of sulfur into the hollow core through the porous shell of the carbon particles, as well as the facilitated electrolyte access of the porous shell through pores of size 2−4 nm.[29] Such hypothesis was not different from the previous physical restraint methods. The great performance of their cathode actually could be explained by our hypothesis: The in-depth sulfur incorporation was enabled by the "sulfur vapor infusion" technique used, although detailed description was not available, which could be speculated as a similar method used in our study. Through sulfur vapor infusion, S_6 or S_2 small molecules at high temperature were capable of diffusing through a narrow pore channel in the shell into a hollow core and change them back to a more stable S_8 with a large molecule size. However, the small size of the narrow pore channel in a carbon shell can effectively prevent the liquid electrolyte penetration and avoid polysulfide dissolution.

■ ASSOCIATED CONTENT

Supporting Information. Additional figures showing the synthesizing process, an HRTEM inage of a disordered nanotube, spectrum of SDNCT-500, and cyclic voltammetry scans of SDCNT and table of element composition in EDS analysis. This material is available free of charge via the Internet at http://pubs.acs.org.

■ AUTHOR INFORMATION

Corresponding Author
*E-mail: cswang@umd.edu.

■ ACKNOWLEDGMENT

This work is supported as part of the Nanostructures for Electrical Energy Storage, an Energy Frontier Research Center funded by the U.S. Department of Energy, Office of Science, Office of Basic Energy Sciences under Award Number DESC0001160. Financial support in part by the Exploratory Technology Research, Vehicle Technologies Program at DoE through National Energy Technology Laboratory (RES1100534) is gratefully acknowledged. We also acknowledge the technical support of the Maryland NanoCenter and its NispLab. The NispLab is supported in part by the National Science Foundation as a MRSEC Shared Experimental Facility. We are especially grateful to Professor Bryan Eichhorn at the Chemistry Department at UMD for his technical support on sealing vacuum quartz tubes.

■ REFERENCES

(1) Tarascon, J. M. *Nature* **2001**, *414*, 359–367.
(2) Whittingham, M. S. *Chem. Rev.* **2004**, *104*, 4271–4301.
(3) Goodenough, J. B.; Kim, Y. *Chem. Mater.* **2010**, *22*, 587–603.
(4) Peled, E.; Yamin, H. *Prog. Batteries Sol. Cells* **1984**, *5*, 56–58.
(5) Kumaresan, K.; Mikhaylik, Y.; White, R. E. *J. Electrochem. Soc.* **2008**, *155*, A576–A582.
(6) Rauh, R. D.; Abraham, K. M.; Pearson, G. F.; Surprenant, J. K.; Brummer, S. B. *J. Electrochem. Soc.* **1979**, *126*, 523–527.
(7) Peled, E.; Sternberg, Y.; Gorenshtein, A.; Lavi, Y. *J. Electrochem. Soc.* **1989**, *136*, 1621–1625.
(8) Shim, J.; Striebel, K. A.; Cairns, E. J. *J. Electrochem. Soc.* **2002**, *149*, A1321–A1325.
(9) Mikhaylik, Y. V.; Akridge, J. R. *J. Electrochem. Soc.* **2003**, *150*, A306–A311.
(10) Cheon, S.; et al. *J. Electrochem. Soc.* **2003**, *150*, A800–A805.
(11) Ryu, H.; et al. *J. Power Sources* **2006**, *163*, 201–206.
(12) Shin, J. H.; Cairns, E. J. *J. Electrochem. Soc.* **2008**, *155*, A368–A373.
(13) Akridge, J. R.; Mikhaylik, Y. V.; White, N. *Solid State Ionics* **2004**, *175*, 243–245.

(14) Mikhaylik, Y. V.; Akridge, J. R. *J. Electrochem. Soc.* **2004**, *151*, A1969–A1976.
(15) Rao, B. M. L.; Shropshire, J. A. *J. Electrochem. Soc.* **1981**, *128*, 942–945.
(16) Choi, Y.; et al. *J. Power Sources* **2008**, *184*, 548–552.
(17) Zheng, W.; Liu, Y. W.; Hu, X. G.; Zhang, C. F. *Electrochim. Acta* **2006**, *51*, 1330–1335.
(18) Choi, Y.; Kim, K.; Ahn, H.; Ahn, J. *J. Alloys Compd.* **2008**, *449*, 313–316.
(19) Yuan, L.; Yuan, H.; Qiu, X.; Chen, L.; Zhu, W. *J. Power Sources* **2009**, *189*, 1141–1146.
(20) Cao, Y.; et al. *Phys. Chem. Chem. Phys.* **2011**, *13*, 7660–7665.
(21) Marmorstein, D.; et al. *J. Power Sources* **2000**, *89*, 219–226.
(22) Hassoun, J.; Scrosati, B. *Angew. Chem., Int. Ed.* **2010**, *49*, 2371–2374.
(23) Wang, J.; et al. *Carbon* **2008**, *46*, 229–235.
(24) Ji, X.; Lee, K.; Nazar, L. F. *Nat. Mater.* **2009**, *8*, 500–506.
(25) Liang, C.; Dudney, N. J.; Howe, J. Y. *Chem. Mater.* **2009**, *21*, 4724–4730.
(26) Lai, C.; Gao, X. P.; Zhang, B.; Yan, T. Y.; Zhou, Z. *J. Phys. Chem. C* **2009**, *113*, 4712–4716.
(27) Yang, Y.; et al. *Nano Lett.* **2010**, *10*, 1486–1491.
(28) Zhang, B.; Qin, X.; Li, G. R.; Gao, X. P. *Energy Environ. Sci.* **2010**, *3*, 1531–1537.
(29) Jayaprakash, N.; Shen, J.; Moganty, S. S.; Corona, A.; Archer, L. A. *Angew. Chem., Int. Ed.* **2011**, *50*, 5904–5908.
(30) Ji, X.; Evers, S.; Black, R.; Nazar, L. F. *Nat. Commun.* **2011**, *2*, 325.
(31) Han, S.; et al. *J. Alloys Compd.* **2003**, *349*, 290–296.
(32) He, X.; et al. *Electrochim. Acta* **2007**, *52*, 7372–7376.
(33) Chen, J.; Shin, K.; Leiston-Belanger, J. M.; Zhang, M.; Russell, T. P. *Adv. Funct. Mater.* **2006**, *16*, 1476–1480.
(34) *Environmental Separation of Heavy Metals - Engineering Processes*; SenGupta, A. K., Ed.; Lewis Publishers: Boca Raton, FL 2002.
(35) Yang, H.; Wen, H.; Zhao, Z.; Li, S. *Chin. Phys. Lett.* **2001**, *18*, 1648–1650.
(36) Kurmaev, E. Z.; Galakhov, A. V.; Moewes, A.; Moehlecke, S.; Kopelevich, Y. *Phys. Rev. B* **2002**, *66*, 193402.
(37) Gupta, S.; Weiner, B. R.; Morell, G. *J. Appl. Phys.* **2002**, *92*, 5457–5462.
(38) Korpiel, J. A.; Vidic, R. D. *Environ. Sci. Technol.* **1997**, *31*, 2319–2325.
(39) *The sulfur data book*; Tuller, W. N., Ed.; McGraw-Hill Book Company, Inc.: New York, 1954.
(40) *Mechanisms of sulfur reactions*; Pryor, W. A.; Ed.; McGraw-Hill Book Company, Inc.: New York, 1962.
(41) Daza, L.; Mendioroz, S.; Pajares, J. A. *Clays Clay Miner.* **1991**, *39*, 14.
(42) Yamin, H.; Gorenshtein, A.; Penciner, J.; Sternberg, Y.; Peled, E. *J. Electrochem. Soc.* **1988**, *135*, 1045–1048.

Supporting Information

Sulfur Impregnated Disordered Carbon Nanotubes Cathode for Lithium-Sulfur Batteries

*Juchen Guo, Yunhua Xu, Chunsheng Wang **

Figure S1. Process of synthesizing sulfur impregnated disordered carbon nanotubes.

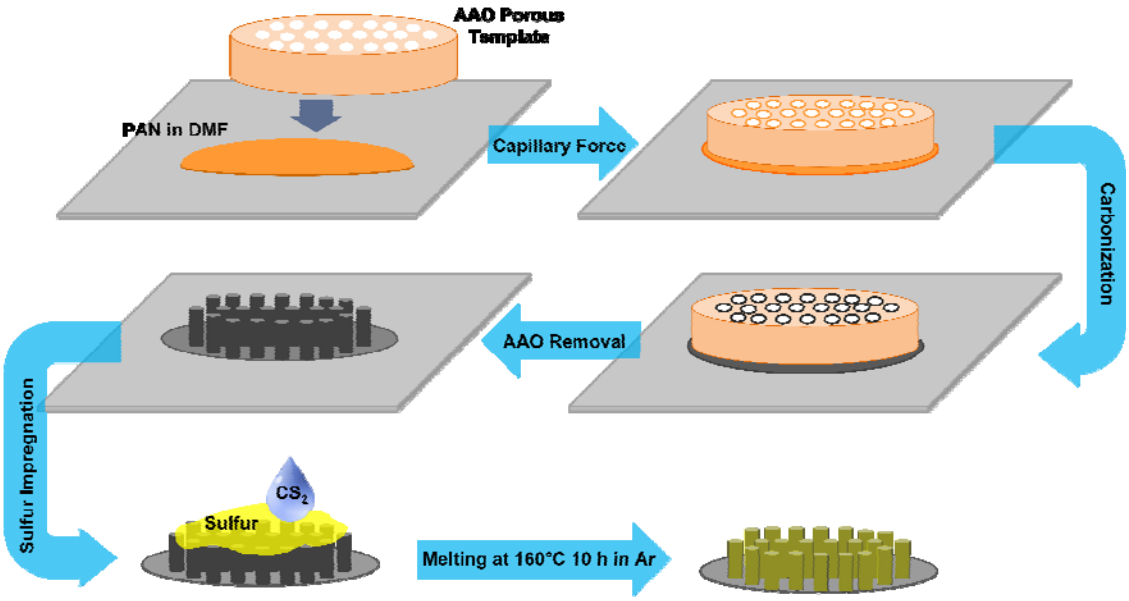

Figure S2. HRTEM image of the disordered carbon nanotube.

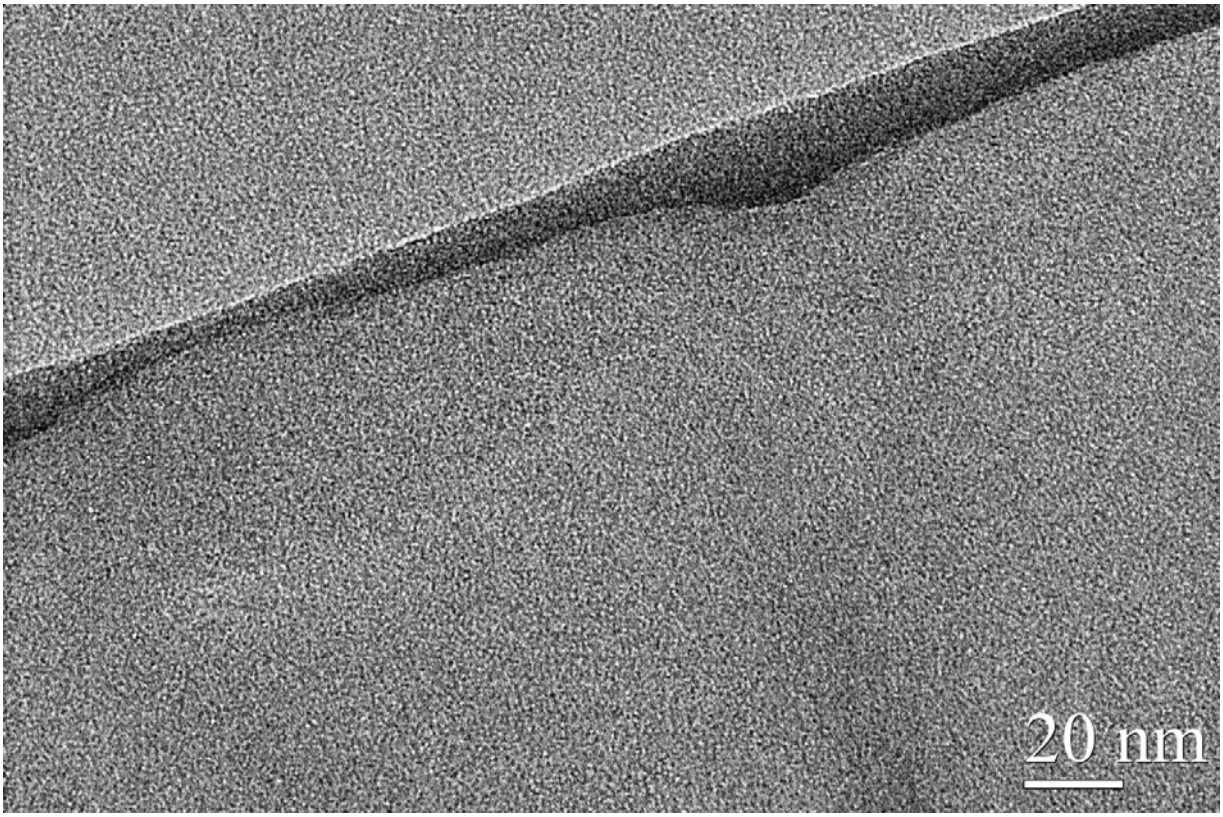

Figure S3. (a) The sum spectrum of SDNCT-500 on TEM gird (silicon monoxide film on Cu grid), and (b) comparison of sulfur and carbon signals.

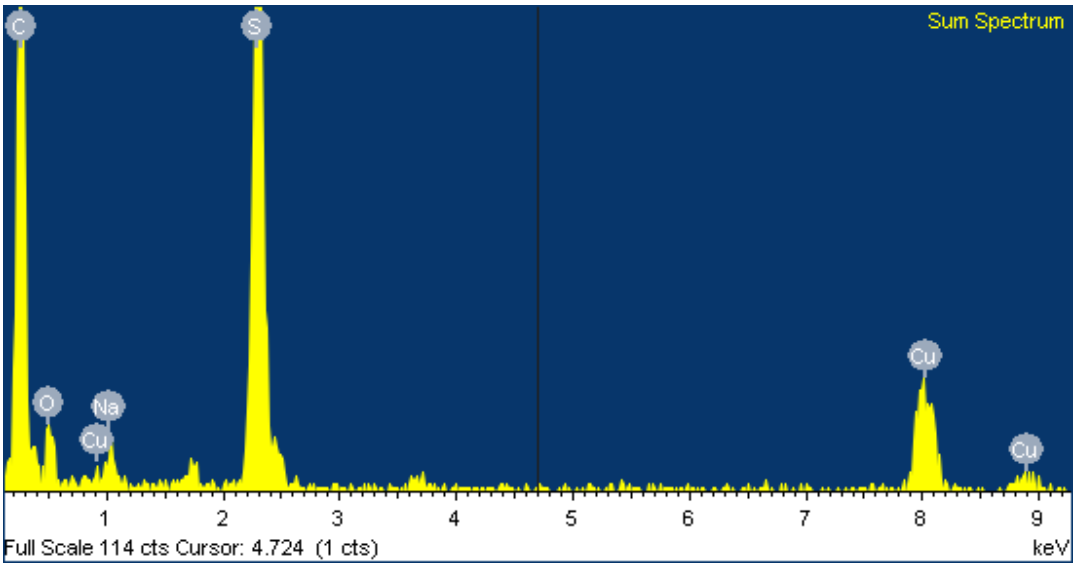

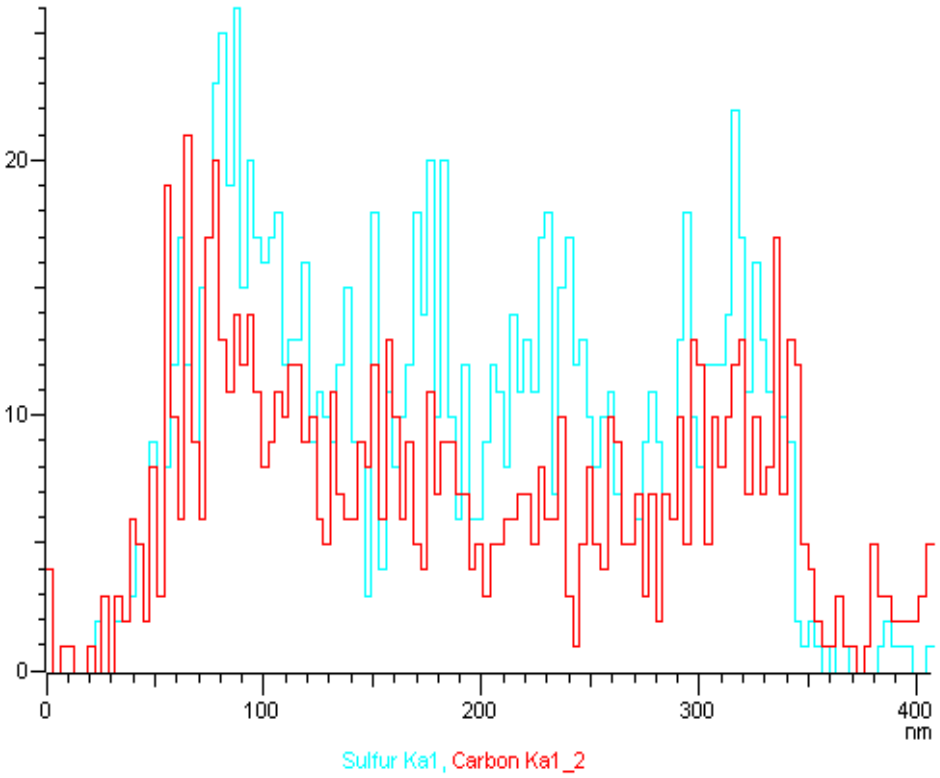

Table S1. Element composition in the EDS analysis

Element	Atomic %	Weight %
Carbon	71.2	47.6
Sulfur	19.1	34.1
Copper *	3.42	12.1
Oxygen	4.83	4.31
Sodium *	1.48	1.89
Total		100

* Copper signal was due to the Cu grid of the TEM sample holder, the sodium signal was due to the residue of NaOH used to remove the AAO template.

Figure S4. Representative cycles from the continuous cyclic voltammetry scan of SDCNT-160.

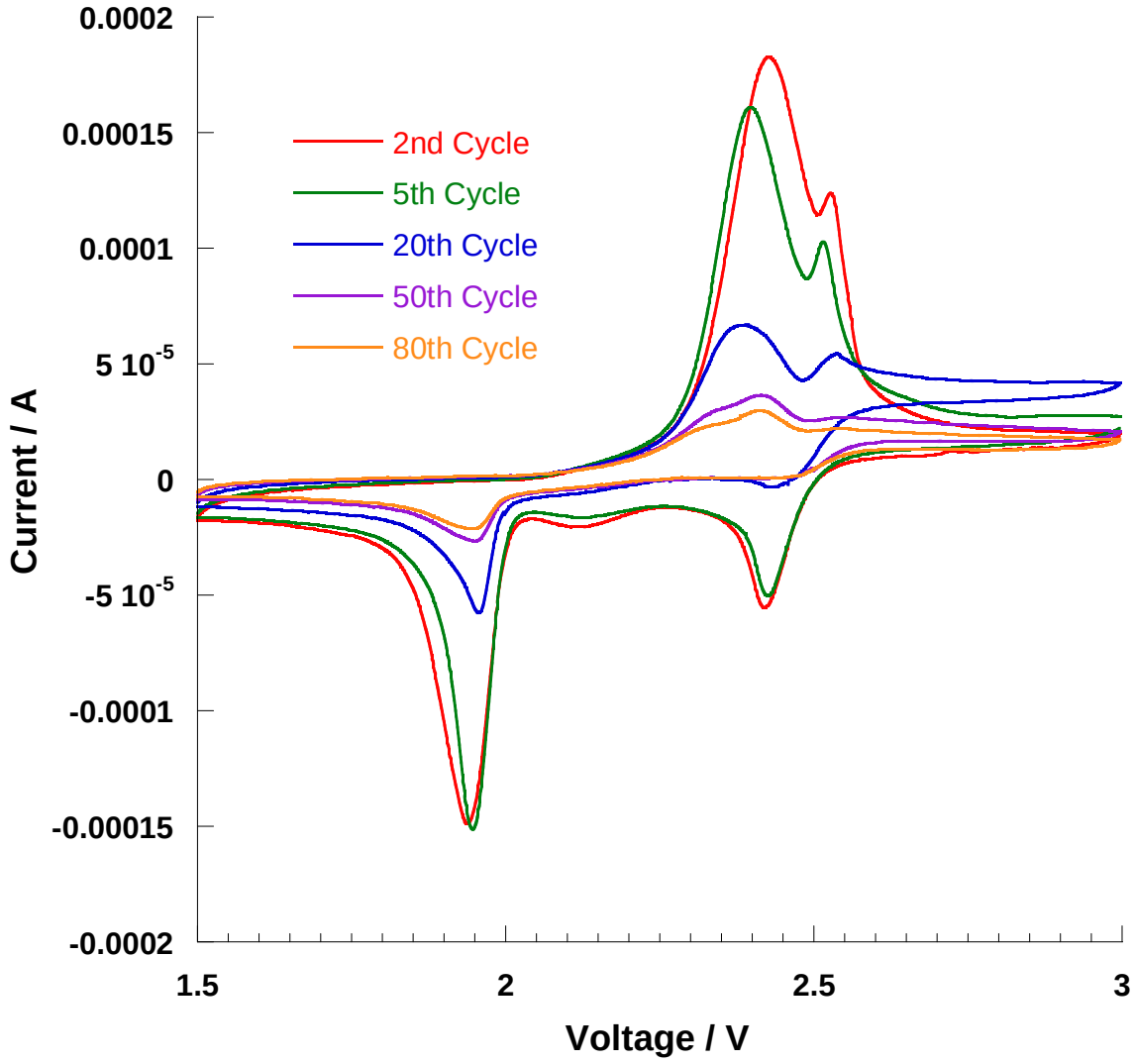

Figure S5. Representative cycles from the continuous cyclic voltammetry scan of SDCNT-300.

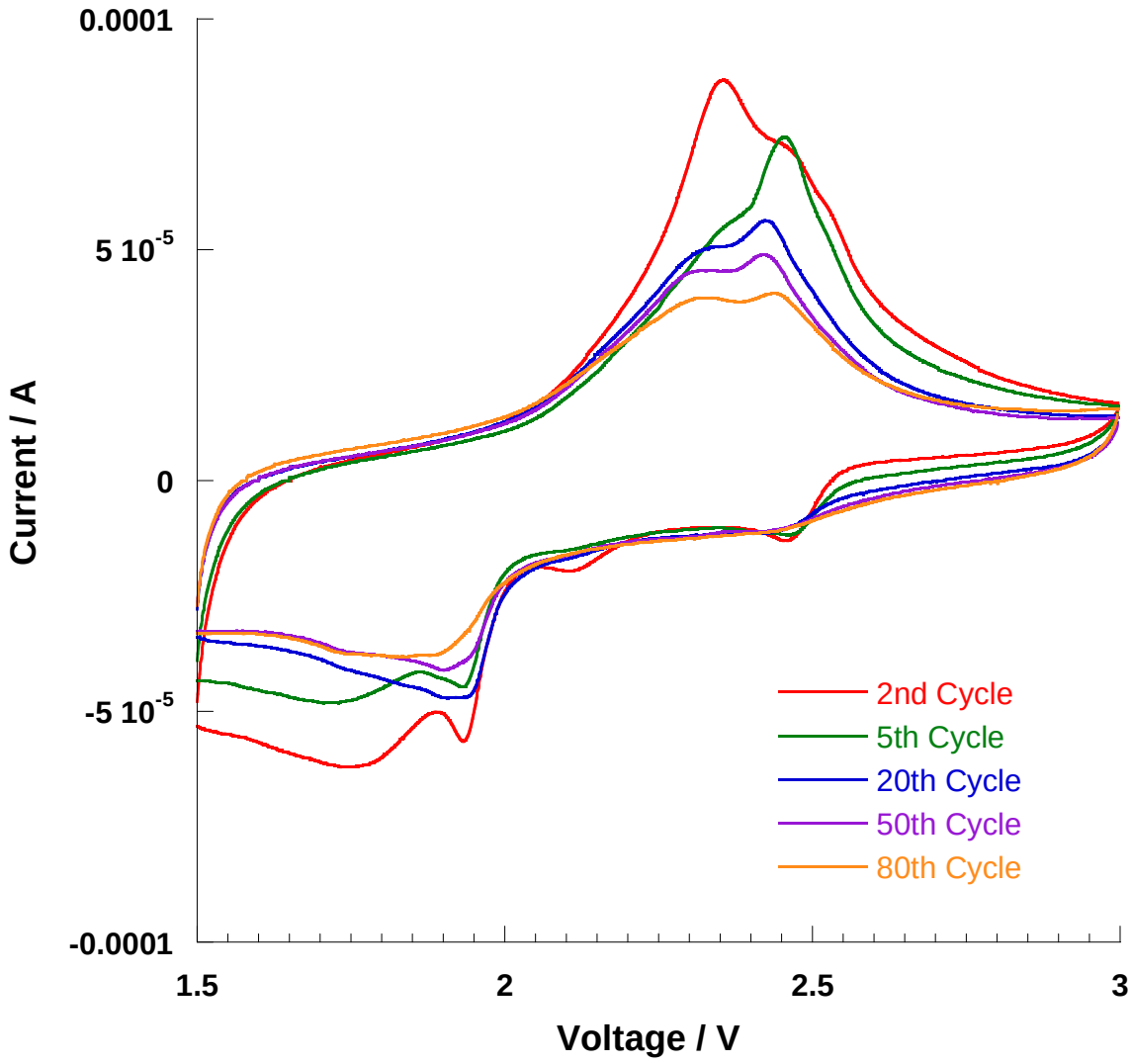

Figure S6. Representative cycles from the continuous cyclic voltammetry scan of SDCNT-500.